Journal of Cardiology 73 (2019) 343–350

Contents lists available at ScienceDirect

Journal of Cardiology

journal homepage: www.elsevier.com/locate/jjcc

Original article

A trafficking-deficient KCNQ1 mutation, T587M, causes a severe phenotype of long QT syndrome by interfering with intracellular hERG transport

Jie Wu (PhD)[a,b,c,1], Tomoko Sakaguchi (MD, PhD)[b,1], Kotoe Takenaka (MD, PhD)[d], Futoshi Toyoda (PhD)[c], Keiko Tsuji (PhD)[b], Hiroshi Matsuura (MD, PhD)[c], Minoru Horie (MD, PhD)[b,*]

[a] Department of Pharmacology, School of Basic Medical Science, Xi'an Jiaotong University Health Science Center, Xi'an, Shaanxi, China
[b] Department of Cardiovascular and Respiratory Medicine, Shiga University of Medical Science, Otsu, Japan
[c] Department of Physiology, Shiga University of Medical Science, Otsu, Japan
[d] Department of Cardiovascular Medicine, Kyoto University Graduate School of Medicine, Kyoto, Japan

ARTICLE INFO

Article history:
Received 30 May 2018
Received in revised form 11 September 2018
Accepted 24 October 2018
Available online 24 December 2018

Keywords:
Long QT syndrome
KCNQ1-T587M
hERG
Fluorescence resonance energy transfer
Patch-clamp

ABSTRACT

Background: KCNQ1-T587M is a C-terminal mutation correlated with severe phenotypes of long QT syndrome (LQTS). However, functional analysis of KCNQ1 channels with the T587M mutation showed a mild genotype in the form of haploinsufficiency in a heterologous expression system. This study sought to explore the molecular mechanism underlying the phenotype–genotype dissociation of LQTS patients carrying the KCNQ1-T587M mutation.

Methods: cDNAs for wild-type (WT) and KCNQ1 mutations (R259C and T587M) were transiently transfected into HEK293 cells stably expressing hERG (hERG-HEK), and whole-cell patch-clamp technique was performed to examine the effect of KCNQ1 mutations on I_{Kr}-like currents. In addition, fluorescence resonance energy transfer (FRET) was conducted to demonstrate the molecular interaction between KCNQ1 and hERG when co-expressed in HEK293 cells.

Results: KCNQ1-T587M mutation produced a significant ($p < 0.01$) decrease in I_{Kr}-like tail current densities without affecting the gating kinetics, while KCNQ1-R259C mutation had no significant effect on the I_{Kr}-like tail current densities. Consistent with this result, FRET experiments demonstrated that both KCNQ1-WT and -R259C interacted with hERG in the cytosol and on the plasma membrane; however, the interaction between KCNQ1-T587M and hERG was observed only in the cytosol, and hERG proteins were seldom transported to the cell membrane, suggesting that the KCNQ1-T587M mutation impaired the trafficking of hERG to the cell membrane.

Conclusions: The disruption of hERG trafficking caused by the KCNQ1-T587M mutation is likely the reason why some patients exhibit severe LQTS phenotypes.

Introduction

The congenital long QT syndrome (LQTS) is a cardiac arrhythmia characterized by an abnormality in myocardial repolarization, leading to the QT interval prolongation on the electrocardiogram and a torsade de pointes (TdP) type of ventricular tachycardia. To date, at least 15 genes have been identified to be responsible for 15 subtypes of the syndrome [1,2], with the first two types of LQTS (LQT1 and LQT2, caused by mutations in *KCNQ1* and *KCNH2*, respectively) being the most common. *KCNQ1* and *KCNH2* separately encode α-subunits of slow (I_{Ks}) and rapid (I_{Kr}) components of delayed rectifier potassium (K^+) currents. I_{Ks} and I_{Kr} are the main repolarizing K^+ currents during the plateau and repolarization phases of the cardiac action potential (AP); they play a critical role in maintaining the repolarization reserve [3].

* Corresponding author at: Department of Cardiovascular and Respiratory Medicine, Shiga University of Medical Science, Seta Tsukinowa, Otsu, Shiga 520-2192, Japan .
E-mail addresses: livedoor629@gmail.com, horie@belle.shiga-med.ac.jp (M. Horie).
[1] These authors contributed equally to this manuscript.

https://doi.org/10.1016/j.jjcc.2018.10.011
0914-5087/

KCNQ1 mutant T587M (KCNQ1-T587M) is a C-terminal mutation that was first reported in three Japanese LQT1 patients, showing very severe phenotypes [4]. The same mutation was also found in LQTS patients with a family history of lethal cardiac arrhythmias and sudden death later [5,6]. Though C-terminal KCNQ1 mutations have been shown to lead to mild LQTS phenotypes in general [7,8], T587M has been shown to be associated with severe clinical manifestations. Functional analyses showed a mild genotype in the form of haploinsufficiency in COS7 cells heterologously expressing wild-type (WT) KCNQ1 and KCNQ1-T587M; although, KCNQ1-T587M alone produced no obvious currents due to trafficking defects [4]. It remains unclear why heterozygous KCNQ1-T587M patients exhibited severe clinical manifestations.

There is growing evidence on the molecular interaction between I_{Ks} and I_{Kr} [9–14], which suggests that a mutation in genes encoding the I_{Ks} channel may disrupt I_{Kr} channel function and protein localization. To address the apparent discrepancy between genotype and phenotype in KCNQ1-T587M patients, we hypothesized that the KCNQ1-T587M mutation affects the intracellular processing of hERG, thereby causing fatal LQTS features. After transfecting mutant KCNQ1 (α-subunit of I_{Ks}) and KCNE1 (β-subunit of I_{Ks}) into HEK293 cells stably expressing hERG-WT (hERG-HEK), we characterized the functional consequences of I_{Kr} currents using the whole-cell patch-clamp technique. By using fluorescence resonance energy transfer (FRET) and confocal imaging techniques, we also examined direct interactions between hERG and mutant KCNQ1 co-expressed with KCNE1 in HEK293 cells. The resulting data showed that KCNQ1-T587M decreased I_{Kr} current densities and disrupted hERG protein trafficking to the cell membrane. These findings may explain why patients carrying the KCNQ1-T587M mutation with a mild genotype exhibited a severe LQTS phenotype.

Methods

DNA constructs and stable transfection of HEK293 cells

The complementary deoxyribonucleic acid (cDNA) encoding human KCNQ1-WT (GenBank AF00057) was subcloned into pCI vector (Promega, Madison, WI, USA). *KCNQ1* mutations R259C and T587M were constructed using a QuikChange™ Site-Directed Mutagenesis Kit according to the manufacturer's instructions (Stratagene, La Jolla, CA, USA), and subcloned into pCI vector. As KCNQ1-R259C could be transported to the surface membrane alone and alter voltage-dependent gating of the KCNQ1 channel [15,16], it was employed as a positive control. All mutants were fully sequenced to ensure fidelity. The *KCNE1* cDNA (GenBank M26685) was subcloned into pIRES/CD8 vector. The two expression vectors were generously provided by Dr J. Barhanin (Institut de Pharmacologie Moléculaire et Cellulaire, CNRS, Nice, France).

The KCNH2-WT cDNA (GenBank AF363636) kindly provided by Dr M. Sanguinetti (University of Utah, Salt Lake City, UT, USA) was subcloned into pIRES1hyg vector (Clontech, Mountain View, CA, USA), which contains the hygromycin-resistance gene. Human embryonic kidney (HEK293) cells were cultured in Dulbecco's modified Eagle's medium (DMEM, Invitrogen, Carlsbad, CA, USA) supplemented with 10% fetal bovine serum and antibiotics (100 IU mL^{-1} penicillin and 100 mg mL^{-1} streptomycin) under a humidified atmosphere of 5% CO_2/95% air at 37 °C. To obtain stably transfected cell line, HEK293 cells were transfected with KCNH2-WT using the lipofectamine method according to the manufacturer's instructions (Invitrogen). After selection in 250 μg/m hygromycin B (Invitrogen) for 15–20 days, single colonies were picked and tested for I_{Kr} current. The stably transfected (hERG-HEK) cells were cultured in the DMEM containing 250 μg/mL hygromycin B (Invitrogen).

To reconstitute co-expression of both I_{Ks} and I_{Kr}, 1 μg of *KCNQ1* (WT or mutants) and 0.5 μg of green fluorescent protein (GFP) were transiently transfected into hERG-HEK cells with or without 1.0 μg of *KCNE1*, using the lipofectamine method.

Electrophysiology and solutions

Forty-eight hours after transfection, cells attached to a glass coverslip were transferred to a 0.5-ml bath chamber perfused with normal Tyrode's solution and maintained at 37 ± 1 °C. Patch-clamp experiments were conducted on GFP-positive cells. The whole-cell membrane current was measured using an EPC-8 amplifier (HEKA, Lambrecht, Germany) with a resistance setting of 2.5–3.5 MΩ.

Currents were induced by depolarizing voltage-clamp steps administered from a holding potential of −80 mV to various test potentials. Amplitudes of currents were determined by measuring the amplitude of the tail current. All currents were normalized to the cell membrane capacitance to obtain current densities (p*A*/p*F*). The voltage-dependence of current activation was determined by fitting the normalized tail current (I_{tail}) versus test potential (V_t) to a Boltzmann function expressed by $I_{tail} = 1/(1 + \exp[(V_{0.5} - V_t)/k])$, where $V_{0.5}$ is the voltage at which the current is half-maximally activated and k is the slope factor.

The normal Tyrode's solution contained 140 mM NaCl, 5.4 mM KCl, 1.8 mM $CaCl_2$, 0.5 mM $MgCl_2$, 0.33 mM NaH_2PO_4, 5.5 mM glucose, and 5 mM HEPES (pH adjusted to 7.4 with NaOH). The pipette solution contained 70 mM potassium aspartate, 40 mM KCl, 10 mM KH_2PO_4, 5 mM EGTA, 1 mM $MgSO_4$, 3 mM Na_2-ATP (Sigma, Tokyo, Japan), 0.1 mM Li_2-GTP, and 5 mM HEPES (pH adjusted to 7.4 with KOH). I_{Kr} blocker E-4031 (Wako, Osaka, Japan) was dissolved in distilled water to yield a 3-mM stock solution. I_{Ks} blocker HMR1556 (a kind gift from Aventis Pharma Deutschland GmbH, Frankfurt, Germany) was dissolved in dimethyl sulfoxide (DMSO, Sigma) to yield a 10-mM stock solution. Both stock solutions were kept at −20 °C.

Fluorescence resonance energy transfer

FRET imaging has been proven to be a powerful tool for detecting protein-protein interactions in living cells [11,17]. To examine the KCNQ1-hERG protein interaction, cyan fluorescent protein (CFP)-tagged *KCNQ1* for WT, R259C, and T587M and yellow fluorescent protein (YFP)-tagged *KCNH2* were constructed using ECFP-N1 and EYFP-N1 vectors (Clontech), respectively. Then, 1.0 μg of CFP-tagged *KCNQ1* (WT and mutants), 1.0 μg of *KCNE1*, and 1.0 μg of YFP-tagged *KCNH2* were transiently co-transfected into HEK 293 cells using lipofectamine. Forty-eight hours after transfection, FRET experiments were performed at room temperature.

Localizations of CFP-tagged and YFP-tagged proteins were detected using a laser-scanning confocal microscope (Zeiss LSM510 META, Berlin, Germany) equipped with a 63×/1.40 numerical aperture oil-immersion objective, a polychrome V illumination source, and a photodiode-based dual emission photometry system. FRET was conducted by acceptor photobleaching and spectral unmixing as described previously [18] with minor modifications, where an increase in CFP signal (dequenching) during incremental photobleaching of YFP can be observed. YFP photobleaching was performed using the 100-W mercury lamp of the microscope with a standard YFP filter cube for 5 min, which was sufficient to photobleach >80% of YFP fluorophores and result in negligible photobleaching of CFP fluorophores. Samples were excited with a 458-nm line of an argon laser at a frequency of 2–20 Hz. The subsequent emitted fluorescence from CFP and YFP was simultaneously collected using a dual emission photometry system.

Confocal images were obtained before and after acceptor photobleaching (a 514-nm line of an argon laser was used to photobleach YFP) using a 458–514-nm dichroic beam splitter with the META detector set between 473 and 558 nm. The two temporally averaged 3D image sets (x, y, and spectrum) were linearly unmixed, resulting in four 2D fluorescence data sets (donor/acceptor and before/after photobleaching). Finally, subtracting the unmixed donor emission before photobleaching from that after photobleaching resulted in the net FRET distribution. FRET efficiency (E) was calculated as,

$$E(\%) = \frac{I_D - I_{DA}}{I_{DA}}$$

where I_{DA} and I_D are the CFP-normalized fluorescence intensities before and after photobleaching of the acceptor (YFP), respectively. The %FRET was calculated by drawing regions of interest (ROI) around the area of the cell and subtracting the background from a cell-free region for each image.

Statistical analysis

All data are expressed as mean ± SEM. Multiple comparisons among groups were carried out using one-way ANOVA, with Bonferroni's least significant difference as the *post hoc* test. A p-value of <0.05 was considered as statistically significant.

Results

Co-expression of KCNQ1-T587M in hERG-HEK cells reduced I_{Kr}-like currents

To assess the functional interactions between hERG and KCNQ1, we measured the membrane currents produced by the expression of WT or mutant KCNQ1 in hERG-HEK cells using whole-cell patch-clamp configuration. Fig. 1 shows representative whole-cell current traces induced by depolarizing voltage-clamp steps given from a holding potential of −80 mV to various test potentials (−60 to +40 mV) in 10-mV increments for 2 s, followed by repolarizing to −60 mV for 2 s (inset, Fig. 1A-a). As shown in Fig. 1A-a, the amplitude of outward currents in hERG-HEK cells were increased with depolarizations of up to 0 mV, but progressively decreased with further depolarizations, which is typical for an inwardly rectifying property of I_{Kr} channels [19]. The cells were then exposed to 1 μM HMR1556 (Fig. 1A-b) to detect KCNQ1 currents, and subsequently to 3 μM E-4031 in the presence of HMR1556 (Fig. 1A-c), to identify I_{Kr} currents. Fig. 1A-d and A-e illustrates the HMR1556-sensitive and E-4031-sensitive currents, respectively, obtained by the digital subtraction of current traces in the absence and presence of each drug. As expected, the E-4031-sensitive currents (Fig. 1A-e), but not the HMR1556 sensitive currents (Fig. 1A-d), could be detected in hERG-HEK cells, confirming that hERG-HEK cells expressed I_{Kr} channels but not KCNQ1 channels. It should be noted that small amounts of outward currents that slowly decayed during depolarizing steps remained even in the presence of HMR1556 and E4031 (Fig. 1A-c), appearing to be due to the endogenous expression of voltage-dependent outward currents in HEK293 cells. In the present study, KCNQ1 (or I_{Ks}-like) and I_{Kr}-like currents are defined as the HMR1556-sensitive and E4031-sensitive tail currents, respectively.

HERG-HEK cells transfected with KCNQ1-WT and -R259C (Fig. 1B and C) exhibited time-dependent outward currents having properties of the KCNQ1 channel in addition to those of the I_{Kr} channel; however, they did not alter the I_{Kr} current densities (Fig. 1B-e and C-e). In contrast, cells co-expressing KCNQ1-T587M

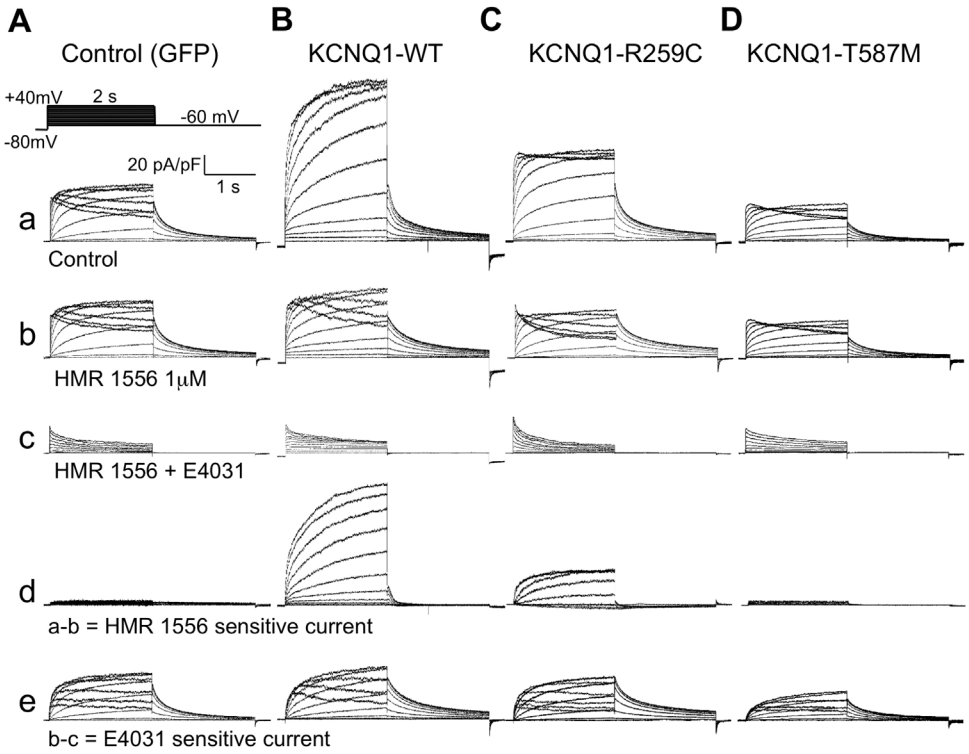

Fig. 1. Co-expression of KCNQ1-T587M reduced I_{Kr} currents in HEK cells stably expressing hERG (hERG-HEK). Representative current traces recorded from hERG-HEK cells expressing green fluorescent protein (GFP) (control, A), KCNQ1-WT (B), KCNQ1-R259C (C), and KCNQ1-T587M (D). After a recording without drugs (a), the cells were externally perfused with 1 μM HMR 1556 (b) and KCNQ1 currents were defined as the HMR 1556-sensitive currents (d). After HMR 1556 application, the cells were further perfused with 3 μM E-4301 (c) and I_{Kr} (hERG) currents were defined as E4301-sensitive currents (e). Currents were elicited using the voltage protocol shown in the inset of panel A-a.

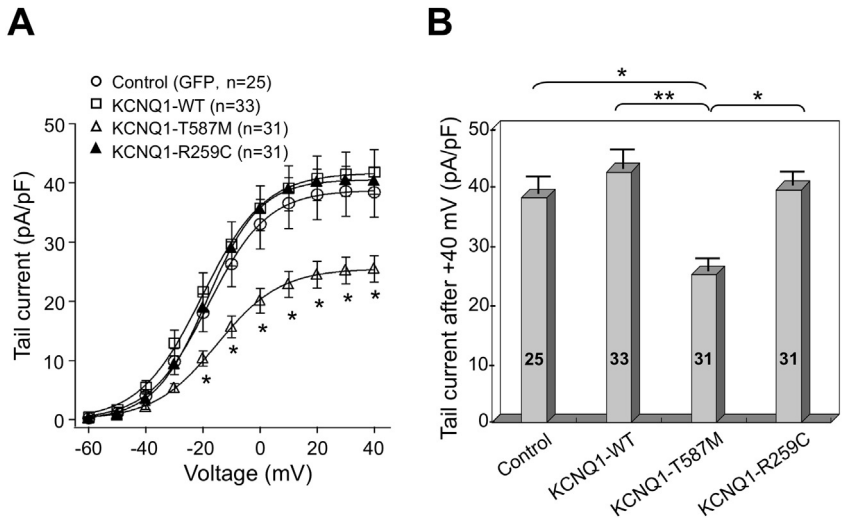

Fig. 2. Co-expression of KCNQ1-T587M reduced I_{Kr} densities without affecting voltage-dependent gating of I_{Kr} channels in hERG-HEK cells. (A) *I–V* relations of E4031-sensitive I_{Kr} in hERG-HEK cells expressing KCNQ1. Open circles: control (GFP), open squares: KCNQ1-WT, open triangles: KCNQ1-T587M, and closed triangles: KCNQ1-R259C. Currents were measured at −60 mV repolarization after various test potentials ranging from −60 to +40 mV. (B) Mean peak I_{Kr} densities of control, KCNQ1-WT, KCNQ1-T587M, and KCNQ1-R259C. $^{*}p < 0.05$ vs. control, $^{**}p < 0.01$ vs. control.

displayed no KCNQ1 currents (Fig. 1D-d) and significantly decreased the I_{Kr} current densities (Fig. 1D-e).

Peak amplitudes of I_{Kr} tail currents (Fig. 1A-e, B-e, C-e) that were elicited on repolarization to −60 mV from various test potentials were measured and normalized to the cell capacitance. These values were plotted as a function of test potentials under four different experimental conditions (Fig. 2A). Open circles indicate mean tail current densities measured from the hERG-HEK cells, in which only GFP was transfected (control), open squares indicate mean tail current densities from the cells with additional KCNQ1-WT, open triangles indicate mean tail current densities with additional KCNQ1-T587M, and closed triangles indicate mean tail current densities with additional KCNQ1-R259C. These data were fitted with a Boltzmann equation and yielded half maximum activation potentials ($V_{0.5}$) and slope factors (k) that were not significantly different (Table 1). Fig. 2B depicts the I_{Kr} current densities after +40 mV test potential. The values of the four groups were found to be significantly different ($p < 0.01$), and the I_{Kr} current density of KCNQ1-T587M was significantly smaller than those of the other 3 groups ($p < 0.01$ vs. control, KCNQ1-WT and KCNQ1-R259C, respectively). Therefore, co-expression with KCNQ1-T587M caused a reduction in the I_{Kr} current without changing the activation parameters.

The time course for deactivation was evaluated (Table 1). There were no significant differences in the deactivation time constants upon repolarization to −60 mV after a 2-s depolarization to +10 mV between cells with and without WT and mutant KCNQ1, indicating that KCNQ1-T587M had no effect on the deactivation.

In another set of experiments, KCNE1 was co-expressed with WT and mutant KCNQ1 in hERG-HEK cells. Fig. 3 shows representative whole-cell current traces recorded from hERG-HEK cells expressing KCNQ1/KCNE1. Fig. 4 and Table 2 show current–voltage (*I–V*) relation curves and activation/deactivation parameters for I_{Kr} tail currents in Fig. 3A-e, B-e, C-e, and D-e. Similar to the data obtained in Figs. 1 and 2, KCNQ1-T587M/KCNE1 co-expression significantly reduced the I_{Kr} tail current density compared to those in the control (GFP/KCNE1), KCNQ1-WT/KCNE1, and KCNQ1-R259C/KCNE1 ($p < 0.01$ vs. control, KCNQ1-WT/KCNE1, and KCNQ1-R259C/KCNE1, respectively), without affecting voltage-dependent gating of I_{Kr} channels (Table 2). In conclusion, KCNQ1-T587M caused a decrease in I_{Kr} current densities regardless of KCNE1.

Direct interaction between hERG and KCNQ1

The results presented above suggest that T587M, a trafficking-deficient KCNQ1 mutation, may affect the intracellular processing of hERG protein. To detect the interaction between KCNQ1 and hERG, we performed a FRET experiment with an acceptor photobleaching technique [11]. Fig. 5A illustrates the

Table 1
Parameters of activation and deactivation of E4031-sensitive I_{Kr} currents in hERG-HEK cells expressing KCNQ1.

Parameters	*n*	Peak tail current (pA/pF)	Activation (mV)		Deactivation		
			$V_{0.5}$	k	τ_f (ms)	τ_s (ms)	$A_f/(A_f+A_s)$
Control (GFP)	32	39.7 ± 2.3	−16.9 ± 1.1	10.5 ± 0.4	320 ± 15	1735 ± 102	0.63 ± 0.01
KCNQ1-WT	33	43.3 ± 2.4	−17.2 ± 1.3	11.0 ± 0.6	323 ± 15	1999 ± 128	0.61 ± 0.01
KCNQ1-R259C	31	43.4 ± 1.8	−17.7 ± 1.1	12.0 ± 0.4	329 ± 11	2098 ± 114	0.65 ± 0.01
KCNQ1-T587M	31	27.2 ± 1.8**,§§,††	−16.3 ± 1.1	10.6 ± 0.5	315 ± 16	1803 ± 120	0.61 ± 0.02

$A_f/(A_f+A_s)$, fractional contribution of τ_f to activation process; $V_{0.5}$, half-maximum activation voltage; k, slope factor; n, number of experiments; τ_f, fast time constant of deactivation; τ_s, slow time constant of deactivation.
** $p < 0.01$ vs. control.
§§ $p < 0.01$ vs. KCNQ1-WT.
†† $p < 0.01$ vs. KCNQ1-R259C.

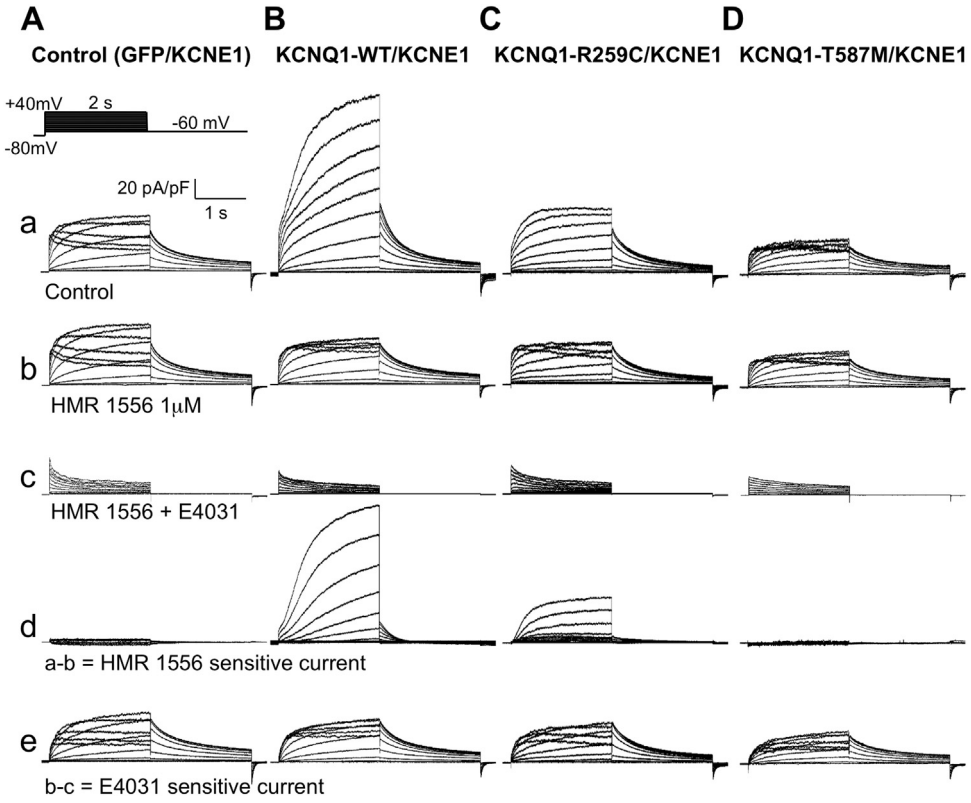

Fig. 3. Co-expression of KCNQ1-T587M/KCNE1 reduced I_{Kr} currents in hERG-HEK cells. Representative current traces recorded from hERG-HEK cells expressing GFP (control, A), KCNQ1-WT/KCNE1 (B), KCNQ1-R259C/KCNE1 (C), and KCNQ1-T587M/KCNE1 (D). Cells were treated with the same protocol as those shown in Fig. 1A-e. Currents were elicited by using the voltage protocol shown in the inset of panel A-a.

confocal microscopic images obtained from HEK293 cells co-expressing KCNE1 and YFP-tagged hERG together with CFP-tagged KCNQ1-WT (top row), CFP-tagged KCNQ1-R259C (second row), and CFP-tagged KCNQ1-T587M (third row), respectively. Panels of the bottom row depict those obtained from cells transfected with CFP and YFP not fused with ion channel genes (negative control).

When performing acceptor photobleaching, the increase in CFP fluorescence intensity (emission spectra ~500 nm) after YFP photobleaching indicates that KCNQ1 physically interacts with

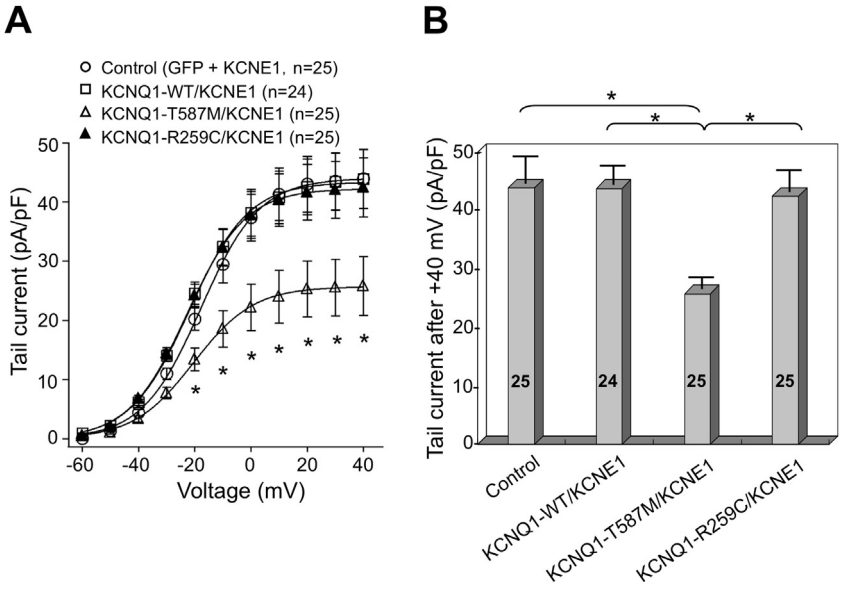

Fig. 4. Co-expression of KCNQ1-T587M/KCNE1 in hERG-HEK cells reduced I_{Kr} densities without affecting voltage-dependent gating of I_{Kr} channels. (A) *I–V* relations of E4031-sensitive I_{Kr} in hERG-HEK cells expressing KCNQ1/KCNE1. Open circles: control (GFP), open squares: KCNQ1-WT/KCNE1, open triangles: KCNQ1-T587M/KCNE1, and closed triangles: KCNQ1-R259C/KCNE1. Currents were measured using the same protocol described in Fig. 2. (B) Mean peak I_{Kr} densities of control, KCNQ1-WT/KCNE1, KCNQ1-T587M/KCNE1, and KCNQ1-R259C/KCNE1. $^{*}p < 0.05$ vs. control, $^{**}p < 0.01$ vs. control.

Table 2
Parameters of activation and deactivation of E4031-sensitive I_{Kr} currents in hERG-HEK cells expressing KCNQ1/KCNE1.

Parameters	n	Peak tail current (pA/pF)	Activation (mV)		Deactivation		
			$V_{0.5}$	k	τ_f (ms)	τ_s (ms)	$A_f/(A_f+A_s)$
Control (GFP)	25	41.4 ± 2.3	−19.8 ± 1.1	10.5 ± 0.4	310 ± 12	1789 ± 80	0.64 ± 0.01
KCNQ1-WT/KCNE1	24	46.3 ± 2.6	−22.2 ± 1.0	11.1 ± 0.5	290 ± 8	1731 ± 72	0.63 ± 0.01
KCNQ1-R259 C/KCNE1	25	44.0 ± 1.8	−18.8 ± 1.5	11.8 ± 0.6	293 ± 10	1746 ± 69	0.66 ± 0.01
KCNQ1-T587 M/KCNE1	25	29.3 ± 1.9**,§§,††	−21.3 ± 1.2	10.8 ± 0.5	292 ± 9	1754 ± 95	0.62 ± 0.01

$A_f/(A_f+A_s)$, fractional contribution of τ_f to activation process; $V_{0.5}$, half-maximum activation voltage; k, slope factor; n, number of experiments; τ_f, fast time constant of deactivation; τ_s, slow time constant of deactivation.
** $p < 0.01$ vs. control.
§§ $p < 0.01$ vs. KCNQ1-WT/KCNE1.
†† $p < 0.01$ vs. KCNQ1-R259C/KCNE1.

hERG. The right panels of Fig. 5A show the fluorescence emission spectra obtained before and after photobleaching in the region of interest (ROI) drawn over the part of the cell (insets of the right panels). In cells co-expressing WT or R259C mutant KCNQ1/KCNE1 with hERG (top and second rows), the YFP-tagged KCNH2 and CFP-tagged KCNQ1 proteins were expressed both in the cytosol and on the plasma membrane. Furthermore, the FRET phenomena, as indicated by the increase in CFP fluorescence, were positive in the ROI drawn over the plasma membrane and the cytosol. In contrast, cells co-expressing KCNQ1-T587M/KCNE1 with hERG (third row) demonstrated intracellular localization of YFP-tagged KCNH2 and CFP-tagged KCNQ1proteins, and FRET was positive in the cytosol. What is more important is that YFP-tagged hERG proteins were seldom distributed on the plasma membrane of cells co-expressing KCNQ1-T587M/KCNE1, suggesting that KCNQ1-T587M impaired the trafficking of hERG to the plasma membrane.

Fig. 5B shows the mean values of FRET efficiency under four different conditions. The FRET efficiency between WT or mutant KCNQ1 and hERG was significantly larger than that of the negative controls ($p < 0.01$ vs. CFP + YFP), indicating the direct interaction between KCNQ1 and hERG.

Discussion

In the present study, we found that KCNQ1-T587M co-expressed with KCNH2 decreased I_{Kr} currents and impaired the intracellular processing of hERG proteins to the cell membrane. The severe phenotype observed in KCNQ1-T587M patients is likely due to the synergistic lesion caused by the KCNQ1-T587M mutation in I_{Ks} and I_{Kr} channels, especially the disruption of hERG trafficking to the cell membrane.

Dissociation between genotypes and phenotypes of KCNQ1-T587M patients

Our previous study on KCNQ1-T587M demonstrated that this mutation failed to cause a proper intracellular processing in the KCNQ1 protein to the cell surface membrane and exerted a mild genotype in the form of haploinsufficiency in a heterologous expression system [4]. Threonine at codon 587 of KCNQ1 is adjacent to a small C-terminal domain (amino acid residues 589–620) that is essential for the channel assembly to form functional tetramers of I_{Ks} [20], suggesting that the T587M variant may fail to associate with WT subunits and therefore exert weak suppression effects on I_{Ks}. Although C-terminal mutations in KCNQ1 were generally reported to cause mild LQTS phenotypes [7,8], our KCNQ1-T587M patients showed severe clinical features. The same mutation was also found in LQTS patients with a family history of lethal cardiac arrhythmias and sudden death [5,6]. Therefore, it remained mysterious why the heterozygous T587M mutation carriers were so severe in phenotypes. The present study offers a potential explanation for the apparent dissociation between genotypes and phenotypes.

Impaired hERG transport may be another molecular mechanism for T587M-related LQTS

An increasing number of studies indicate that KCNQ1 and hERG proteins do physically associate with each other, although the functional outcome from the interaction between the two proteins is still in dispute [9,11–14]. Some studies revealed the I_{Ks}–I_{Kr} interaction through co-immunoprecipitation and electrophysiological analysis on channel functions [13,14]. Using the FRET technique, Organ-Darling et al. confirmed the direct correlations between hERG and KCNQ1 α-subunits in both heterologous and primary cardiomyocytes [11]. Consistent with the study of Organ-Darling et al., our FRET experiment showed that three types of KCNQ1 subunits (WT, R259C, and T587M) all directly interacted with hERG proteins. These studies provide a solid molecular support for the possibility that a KCNQ1 mutation may disrupt the normal function of I_{Kr} encoded by hERG, and vice versa.

In our HEK cells stably expressing hERG, co-expression of KCNQ1-T587M with or without KCNE1 significantly decreased hERG current density (Figs. 1–4). A similar effect caused by another KCNQ1 mutation was also observed in the study by Ren et al. [13], wherein it was shown that transiently expressed KCNQ1 pore mutation Y315S downregulated I_{Kr} in both CHO and HEK 293 cells stably expressing hERG. Nevertheless, co-expression of KCNQ1-T587M did not alter voltage-dependent gating of I_{Kr} channels, suggesting that KCNQ1-T587M may suppress I_{Kr} through disrupting hERG protein trafficking to the cell membrane. Our FRET experiment indicates that KCNQ1-WT and KCNQ1-R259C interacted with hERG both in the cytosol and on the plasma membrane. However, KCNQ1-T587M interacted with hERG only in the cytosol, and hERG proteins were seldom transported to the cell membrane (Fig. 5A) when KCNQ1-T587M and hERG were co-expressed. Consistent with our study, Biliczki et al. found that [21], in western blotting experiments with crude membrane protein extracts, KCNQ1-T587M significantly decreased the KCNH2 plasma membrane protein expression in HEK 293 cells co-transfected with KCNH2-WT + KCNQ1-T587M, compared with those co-transfected with KCNH2-WT + KCNQ1-WT. It is reasonable to conclude that the KCNQ1-T587M mutation prevented hERG trafficking to the cell membrane.

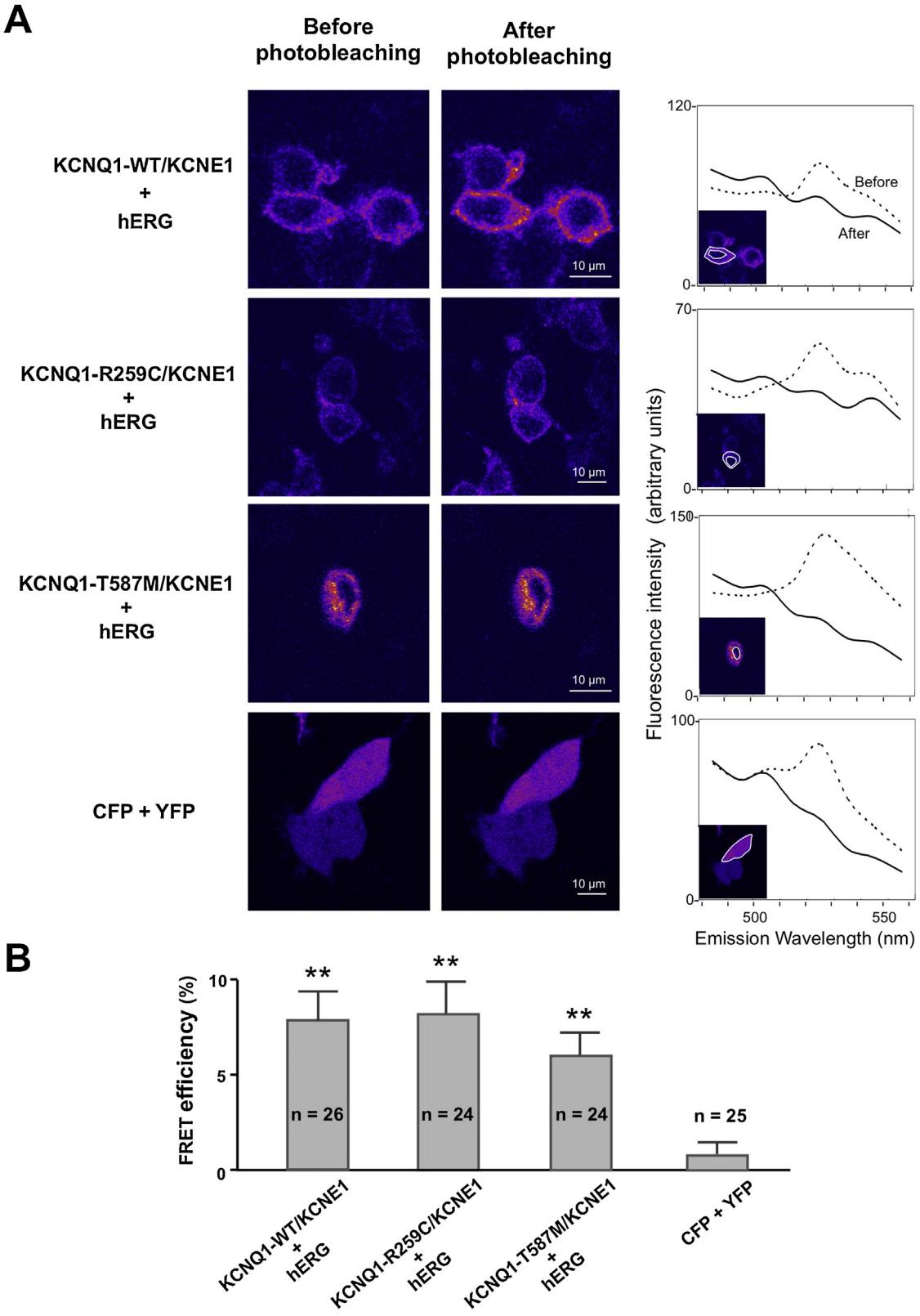

Fig. 5. Fluorescence resonance energy transfer (FRET) analysis confirmed the KCNQ1-hERG interaction and that KCNQ1-T587M disrupted hERG trafficking to the cell membrane. (A) Representative confocal microscopic images of HEK293 cells co-expressing CFP-tagged KCNQ1-WT/KCNE1 + YFP-tagged hERG (top row), CFP-tagged KCNQ1-R259C/KCNE1 + YFP-tagged hERG (second row), CFP-tagged KCNQ1-T587 M + YFP-tagged hERG (third row), and KCNE1 + CFP + YFP (fourth row). The left panels show basal CFP-tagged KCNQ1 fluorescence with excitation at 458 nm and emission at 483 nm. Cells were then exposed to maximal intensity laser light at 514 nm (acceptor photobleaching). The middle panels show corresponding confocal microscopic images after YFP photobleaching. The graphs in the right column show quantification of fluorescence intensity obtained before (dotted line) and after (solid line) photobleaching. The insets in the graphs display the area of the regions of interest (ROI) drawn over the cells. (B) FRET efficiency of KCNE1 + CFP + YFP (control), KCNE1 + KCNQ1-WT + hERG, KCNE1 + KCNQ1-T587 M + hERG, and KCNE1 + KCNQ1-R259C + hERG. $^{**}P < 0.01$ vs. KCNE1 + CFP + YFP.

Conclusion

Our study demonstrates the interaction between KCNQ1 and hERG, and that the KCNQ1-T587M mutation impaired hERG trafficking to the surface cell membrane. These data not only identify an unusual mechanism contributing to the dissociation of genotype–phenotype correlation in LQTS, but also provide new mechanistic insights and implications for the pathogenesis of LQTS caused by the interaction between KCNQ1 and hERG: (1) a mutation in one ion channel gene may disrupt the function of another ion channel encoded by other genes, leading to aberrant clinical manifestations; (2) some *KCNQ1* mutation carriers are emotion-sensitive, while some *KCNH2* mutation carriers are exercise-sensitive; this may be explained by I_{Ks}–I_{Kr} interactions since a *KCNQ1* mutation may disrupt I_{Kr}, and a *KCNH2* mutation may impair I_{Ks} [9]; (3) the synergistic lesion in an ion channel, which is caused by mutations in two genes (i.e. *KCNQ1* and *KCNH2*), is likely one of the possible reasons why a compound LQTS mutation carrier exhibits a more severe phenotype [22]. In a LQTS family harboring three compound mutations, we found that the *KCNH2*-E1039X mutation impaired the I_{Ks} channel in synergy with the disruption caused by KCNQ1-R174C [9], which predisposed compound mutant carriers to a more severe LQTS phenotype.

Limitations

This study was conducted in heterologous expression systems, which may not completely recapitulate the protein trafficking in cardiac myocytes in LQTS patients. Thus further studies are required to confirm the disruption of hERG trafficking caused by the KCNQ1-T587M mutation in native ventricular myocardium.

Funding

This work was supported by the National Natural Science Foundation of China (No. 81273501 and No. 81470378 to JW), a research grant from the Ministry of Education, Culture, Science, and Technology of Japan (to MH) and a health science research grant (H18-Research on Human Genome-002) from the Ministry of Health, Labor and Welfare of Japan (to MH).

Conflicts of interest

The authors declare that there is no conflict of interest.

Acknowledgments

We gratefully acknowledge the technical assistance of Mr. Takefumi Yamamoto (Central Research Laboratory, Shiga University of Medical Science, Otsu, Japan).

References

[1] Bohnen MS, Peng G, Robey SH, Terrenoire C, Iyer V, Sampson KJ, et al. Molecular pathophysiology of congenital long QT syndrome. Physiol Rev 2017;97:89–134.
[2] Schwartz PJ, Ackeman MJ, George AL, Wilde AA. Impact of genetics on the clinical management of channelopathies. J Am Coll Cardiol 2013;62:169–80.
[3] Sanguinetti MC, Long QT. syndrome: ionic basis and arrhythmia mechanism in long QT syndrome type 1. J Cardiovasc Electrophysiol 2000;11:710–2.
[4] Yamashita F, Horie M, Kubota T, Yoshida H, Yumoto Y, Kobori A, et al. Characterization and subcellular localization of KCNQ1 with a heterozygous mutation in the C terminus. J Mol Cell Cardiol 2001;33:197–207.
[5] Furushima H, Chinushi M, Sato A, Aizawa Y, Kikuchi A, Takakuwa K, et al. Fetal atrioventricular block and postpartum augmentative QT prolongation in a patient with long-QT syndrome with KCNQ1 mutation. J Cardiovasc Electrophysiol 2010;21:1170–3.
[6] Chen S, Zhang L, Bryant RM, Vincent GM, Flippin M, Lee JC, et al. KCNQ1 mutations in patients with a family history of lethal cardiac arrhythmias and sudden death. Clin Genet 2003;63:273–82.
[7] Ruwald MH, Xu Parks X, Moss AJ, Zareba W, Baman J, McNitt S, et al. Stop-codon and C-terminal nonsense mutations are associated with a lower risk of cardiac events in patients with long QT syndrome type 1. Heart Rhythm 2016;13:122–31.
[8] Shimizu W, Horie M, Ohno S, Takenaka K, Yamaguchi M, Shimizu M, et al. Mutation site-specific differences in arrhythmic risk and sensitivity to sympathetic stimulation in the LQT1 form of congenital long QT syndrome: multicenter study in Japan. J Am Coll Cardiol 2004;44:117–25.
[9] Wu J, Mizusawa Y, Ohno S, Ding WG, Higaki T, Wang Q, et al. A hERG-E1039X mutation and KCNQ1-R174C mutation produced a synergistic lesion on cardiac I_{Ks} channel in a compound LQTS family. Sci Rep 2018;8:3129.
[10] Kui P, Orosz S, Takacs H, Sarusi A, Csik N, Rarosi F, et al. New in vitro model for proarrhythmia safety screening: I_{Ks} inhibition potentiates the QTc prolonging effect of I_{Kr} inhibitors in isolated guinea pig hearts. J Pharmacol Toxicol Methods 2016;80:26–34.
[11] Organ-Darling LE, Vernon AN, Giovanniello JR, Lu Y, Moshal K, Roder K, et al. Interactions between hREG and KCNQ1 α-subunits are mediated by their COOH termini and modulated by cAMP. Am J Physiol Heart Circ Physiol 2013;304:H589–99.
[12] Guo J, Wang T, Yang T, Xu J, Li W, Fridman MD, et al. Interaction between the cardiac rapidly (I_{Kr}) and slowly (I_{Ks}) activating delayed rectifier potassium channels revealed by low K^+-induced hERG endocytic degradation. J Biol Chem 2011;286:34664–74.
[13] Ren XQ, Liu GX, Organ-Darling LE, Zheng R, Roder K, Jindal HK, et al. Pore mutants of HERG and KvLQT1 downregulate the reciprocal currents in stable cell lines. Am J Physiol Heart Circ Physiol 2010;299:H1525–34.
[14] Ehrlich JR, Pourrier M, Weerapura M, Ethier N, Marmabachi AM, Hébert TE, et al. KvLQT1 modulates the distribution and biophysical properties of HERG. A novel alpha-subunit interaction between delayed rectifier currents. J Biol Chem 2004;279:1233–41.
[15] Kubota T, Shimizu W, Kamakura S, Horie M. Hypokalemia-induced long QT syndrome with an underlying novel missense mutation in S4-S5 linker of KCNQ1. J Cardiovasc Electrophysiol 2000;11:1048–54.
[16] Yagi N, Itoh H, Hisamatsu T, Tomita Y, Kimura H, Fujii Y, et al. A challenge for mutation specific risk stratification in long QT syndrome type 1. J Cardiol 2018;72:56–65.
[17] Zaccolo M. Use of chimeric fluorescent proteins and fluorescence resonance energy transfer to monitor cellular responses. Circ Res 2004;94:866–73.
[18] Gu Y, Di WL, Kelsell DP, Zicha D. Quantitative fluorescence resonance energy transfer (FRET) measurement with acceptor photobleaching and spectral unmixing. J Microsc 2004;215:162–73.
[19] Yang T, Snyders DJ, Roden DM. Rapid inactivation determines the rectification and $[K]_o$ dependence of the rapid component of the delayed rectifier K^+ current in cardiac cells. Circ Res 1997;80:782–9.
[20] Schmitt N, Schwarz M, Peretz A, Abitbol I, Attali B, Pongs O. A recessive C-terminal Jervell and Lange-Nielsen mutation of the KCNQ1 channel impairs subunit assembly. EMBO J 2000;19:332–40.
[21] Biliczki P, Girmatsion Z, Brandes RP, Harenkamp S, Pitard B, Charpentier F, et al. Trafficking-deficient long QT syndrome mutation KCNQ1-T587M confers severe clinical phenotype by impairment of *KCNH2* membrane localization: evidence for clinically significant I_{Kr}–I_{Ks} alpha-subunit interaction. Heart Rhythm 2009;6:1792–801.
[22] Fujii Y, Matsumoto Y, Hayashi K, Ding WG, Tomita Y, Fukumoto D, et al. Contribution of a KCNH2 variant in genotyped long QT syndrome: Romano-Ward syndrome under double mutations and acquired long QT syndrome under heterozygote. J Cardiol 2017;70:74–9.